Research Square

Preprints are preliminary reports that have not undergone peer review.
They should not be considered conclusive, used to inform clinical practice,
or referenced by the media as validated information.

Porous Cellulose/Zn-Containing Composite Aerogel with Zinc Nitrate Hexahydrate as a Hydrated-Salt Phase Change Material: Synthesis Optimization and Thermal Performance

S. Karimnejad
Yadegar-e-Imam Khomeini (RAH) Shahre Rey Branch, Islamic Azad University
M. Hoseinkhani
mhtex92@gmail.com

Yadegar-e-Imam Khomeini (RAH) Shahre Rey Branch, Islamic Azad University
M. Montazer
Amirkabir University of Technology
A. A. Zolriasatein
Yadegar-e-Imam Khomeini (RAH) Shahre Rey Branch, Islamic Azad University
K. Farizadeh
Yadegar-e-Imam Khomeini (RAH) Shahre Rey Branch, Islamic Azad University

Research Article

Keywords: Melting enthalpy, Pore-size distribution, Thermal stability, Cotton fibers, Salt-hydrate dehydration

Posted Date: November 11th, 2026

DOI: https://doi.org/10.21203/rs.3.rs-10632850/v1

License: This work is licensed under a Creative Commons Attribution 4.0 International License.
Read Full License

Additional Declarations: No competing interests reported.

Porous Cellulose/Zn-Containing Composite Aerogel with Zinc Nitrate Hexahydrate as a Hydrated-Salt Phase Change Material: Synthesis Optimization and Thermal Performance

S. Karimnejad[a], M. Hoseinkhani[a,c,*], M. Montazer[b], A. A. Zolriasatein[a], K. Farizadeh[a]

[a] Department of Textile Engineering, Yadegar-e-Imam Khomeini (RAH) Shahre Rey Branch, Islamic Azad University, Tehran, Iran.

[b] Department of Textile Engineering, Amirkabir University of Technology, Tehran, Iran.

[c] Iranian Islamic Fashion and Clothing Research Center, Islamic Azad University, Tehran, Iran.

Corresponding author

M. Hoseinkhani*

Email: **mhtex92@gmail.com**

Abstrac

Hydrated-salt phase change materials are promising candidates for low-temperature thermal energy storage; however, their practical application is often limited by structural instability, salt migration, and insufficient compatibility with supporting matrices. In this study, a freeze-dried porous cellulose/Zn-containing composite incorporating zinc nitrate hexahydrate was developed and optimized as a bio-based support for latent heat storage. The cellulose-derived porous framework provided a scaffold for accommodating and confining Zn-containing species within the composite structure. X-ray diffraction analysis indicated the presence of Zn-containing crystalline phases, while FTIR spectroscopy suggested interactions among the cellulose matrix, nitrate groups, and Zn-containing species. SEM/EDS observations supported the presence and distribution of Zn-containing particulate domains within the cellulose-based scaffold, with feature sizes predominantly in the nanometric range. Thermal analysis showed improved thermal stability compared with neat cellulose, as evidenced by a shift of the main degradation region toward higher temperatures. Differential scanning calorimetry revealed a latent heat storage capacity of 157.1 J/g and a peak melting temperature of 39.05 °C, indicating the suitability of the composite for low-temperature thermal energy storage. Overall, the results suggest that freeze-dried porous cellulose/Zn-containing composites are promising sustainable support materials for hydrated-salt phase change systems, although further porosity, leakage, and thermal cycling studies are required to fully assess long-term practical performance.

Keywords: Cellulose composite; Porous scaffold; Zn-containing species; Zinc nitrate hexahydrate; Phase change material; Thermal energy storage; Latent heat; Thermal stability

1. Introduction:

Aerogels, first pioneered by Kistler in 1931 [1], represent a unique class of ultra-lightweight porous materials. Due to their exceptional properties, including high porosity, significant specific surface area, low dielectric constant, and tunable thermal conductivity, they have attracted considerable attention across various industrial sectors [2–4]. Recent advancements have expanded their application to controlled drug delivery systems [11], high-capacity biosorbents [12], and efficient oil recovery and emulsion separation [13–15].

The versatility of aerogels stems from the diverse range of matrices available, including silica, zirconia, alumina, carbon, and cellulose [16]. Among these, cellulose aerogels have emerged as a sustainable and eco-friendly alternative to synthetic counterparts, owing to the abundance,

renewability, and cost-effectiveness of cellulose [17,18]. These bio-based aerogels have demonstrated significant potential in thermal insulation, advanced electronic components, and biomedical engineering [19–21].

The fabrication of cellulose aerogels typically involves the formation of a hydrogel precursor followed by a drying process to remove the solvent while preserving the porous network. While various drying techniques exist, freeze-drying is frequently employed due to its ability to maintain structural integrity and tailor the morphology of the resulting aerogel [22,25]. Furthermore, recent studies have explored the role of specific solvent systems, such as molten salt hydrates, in the dissolution and regeneration of cellulose to functionalize the aerogel matrix [14,20].

Despite these advancements, there is a growing interest in developing multifunctional cellulose nanocomposites that integrate metallic nanostructures and hydrate salts for enhanced thermal energy storage. In this study, we propose a one-pot synthesis of a cellulose/zinc-containing nanocomposite aerogel via a freeze-drying approach. It is hypothesized that zinc nitrate hexahydrate ($Zn(NO_3)_2{\cdot}6H_2O$) may serve a multi-functional role: (i) as a structural agent for cellulose regeneration, (ii) as a potential precursor for the formation of zinc-based phases within the porous framework, and (iii) as a hydrated salt component for latent heat storage. The primary objective is to investigate the structural, chemical, and thermal properties of the resulting nanocomposites using XRD, FTIR, DSC, SEM-EDS, and TGA, and to evaluate the potential of the cellulose matrix in encapsulating the hydrated salt for thermal management applications.

2. Experimental Section:

2.1. Materials and Reagents:

The primary polysaccharide source used in this study was pharmaceutical-grade hydrophilic cotton cellulose fibers, obtained from Kaveh Co. (Saveh, Iran). According to the manufacturer's specification, the cellulose possessed a high α-cellulose content of >98%(purity), with a weight-average molecular weight **(**Mw**)** of approximately 1.8×10^5g/mol (corresponding to a degree of polymerization of about 1100) [1]. To ensure the removal of any non-cellulosic components such as waxes and pectins, the raw fibers were thoroughly washed with deionized water and NaOH, followed by drying in a vacuum oven at 60 °C for 24 hours. The structural integrity and functional groups of the purified cellulose were verified via FTIR and XRD analysis prior to use. Zinc nitrate hexahydrate ($Zn(NO_3)_2{\cdot}6H_2O$) was purchased from Merck (Darmstadt, Germany), and deionized water was supplied by Zolal Teb Shimi Co. (Tehran, Iran). All chemical reagents were of analytical grade and used as received without further purification.

2.2. Characterization Techniques

The prepared freeze-dried porous cellulose/Zn-containing composites were characterized using complementary analytical techniques to evaluate their structural, chemical, morphological, elemental, and thermal properties. X-ray diffraction (XRD) analysis was carried out using an Equinox 3000 diffractometer (INEL, France) to identify the crystalline phases present in the composites. Fourier-transform infrared (FTIR) spectroscopy was performed using a PerkinElmer Spectrum One instrument (USA) to examine the functional groups and possible interactions among the composite components. The morphology and porous structure of the samples were examined by scanning electron microscopy (SEM) using a Philips XL30 microscope (Netherlands). The elemental composition and distribution of Zn in the composite matrix were analyzed by energy-dispersive X-ray spectroscopy (EDS) using an Oxford Instruments Ultim Max system (UK). Thermogravimetric analysis (TGA) was conducted using a PerkinElmer Diamond instrument (USA) to evaluate the thermal stability and decomposition behavior of the samples. Differential

scanning calorimetry (DSC) measurements were performed using a Netzsch DSC 214 Polyma instrument (Germany) to investigate the thermal transitions and phase change behavior of the hydrated-salt-containing composites.

2.3. Synthesis Procedure

The porous cellulose/Zn-containing composites were prepared through aqueous mixing, gel formation, and subsequent freeze-drying. To optimize the structural and thermal properties of the obtained composites, the effects of key synthesis parameters, including the concentration of zinc nitrate hexahydrate, the cellulose-to-salt ratio, processing temperature, and mixing time, were systematically investigated, as summarized in Table 1 and illustrated in Figure 1. In a typical preparation procedure, predetermined amounts of cotton-derived cellulose were dispersed in an aqueous solution containing zinc nitrate hexahydrate. The mixture was stirred under the selected experimental conditions shown in Table 1, leading to the formation of a cellulose-based hydrogel system. The resulting hydrogels were then subjected to freeze-drying at −50 °C and 0.05 mbar for 24 h to obtain freeze-dried porous composite structures.

Table 1. Experimental design and preparation conditions for the synthesized samples.

Code	Cotton/PCM %w/w	Tempetatuer (°C)	Time (min)
$P_1T_1M_1$	1	75	65
$P_1T_2M_2$	1	85	75
$P_2T_1M_1$	0.7	75	65
$P_2T_2M_2$	0.7	85	75
$P_3T_1M_1$	0.5	75	65
$P_3T_2M_2$	0.5	85	75

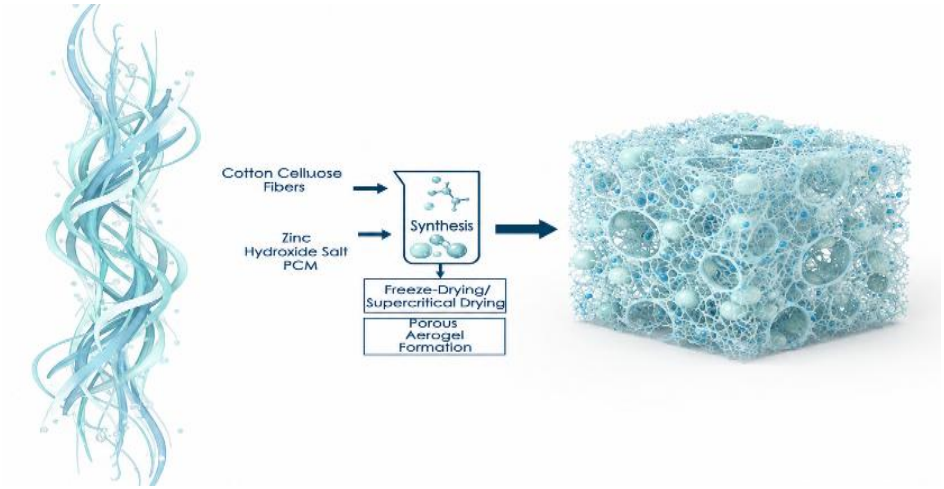


Figure1 . Graphical representation of the preparation of porous cellulose-zinc-PCM nanocomposite aerogels from cotton cellulose fibers.

2.4. Optimization and Characterization

To identify the optimal synthesis condition, all prepared samples were systematically characterized using XRD and FT-IR spectroscopy. The optimal sample, selected based on the structural integrity and chemical interactions confirmed by these analyses, was then subjected to further comprehensive characterization. The morphology, elemental composition, thermal stability, and thermal energy storage capacity of the optimized aerogel were evaluated using SEM, EDS, TGA, and DSC techniques, respectively.

3. Results and discussion:

3.1. Spectrum analysis (FTIR)

FT-IR spectroscopy was used to examine the chemical structure of raw cotton cellulose and the synthesized cellulose/Zn-containing composite samples. The spectra were recorded over the range of 4000–500 $cm^{-1}$for raw cotton cellulose and the prepared samples $P_2T_1M_1$, $P_2T_2M_2$, $P_3T_1M_1$, and $P_3T_2M_2$.The comparative spectra are presented in Figure 2 and Figure 3.

The FTIR spectrum of raw cotton cellulose(Figures 2) exhibited the expected characteristic absorption bands of cellulose. The broad band around 3422 cm^{-1} was attributed to O–H stretching vibrations arising from intra- and intermolecular hydrogen bonding. The band near 2900 cm^{-1} corresponded to C–H stretching vibrations in the polysaccharide backbone, while the absorption band around 1028 $cm^{-1}$was associated with C–O and C–O–C stretching vibrations linked to the β-1,4-glycosidic structure of cellulose. After incorporation of the Zn-containing component, noticeable changes were observed in the FTIR spectra of the composite samples. In particular, the O–H stretching band shifted to higher wavenumbers and its relative intensity decreased, suggesting interactions between cellulose hydroxyl groups and Zn-containing species, likely through coordination and/or hydrogen-bonding interactions. In addition, the attenuation of the cellulose-related band near 1028 cm^{-1} indicates that the local environment of the cellulose network was modified during composite formation. New bands appearing around 1389 cm^{-1} and 1354 cm^{-1} were consistent with nitrate-related vibrations, supporting the presence of zinc nitrate within the cellulose-based structure. A band near 828 cm^{-1} may be associated with Zn–O vibrations.

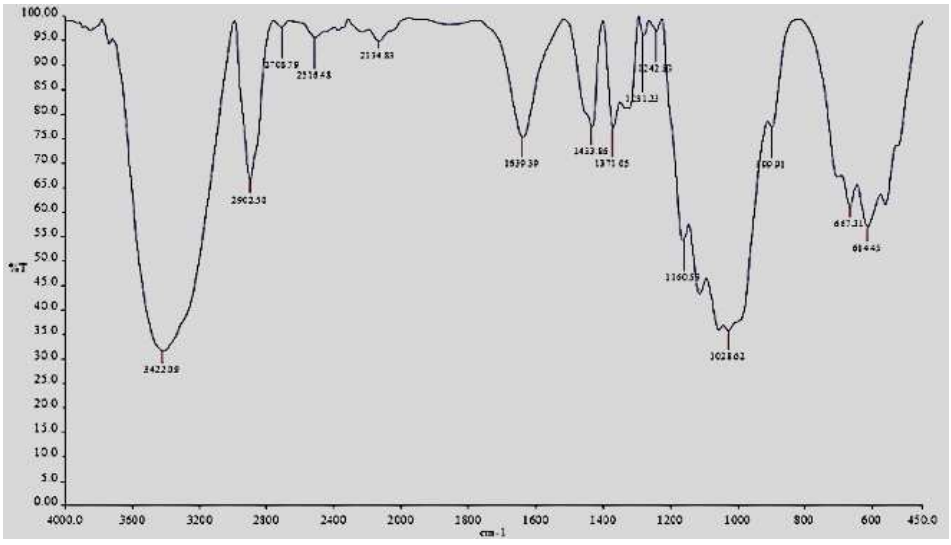


Figure2. FTIR spectrum of raw cotton cellulose.

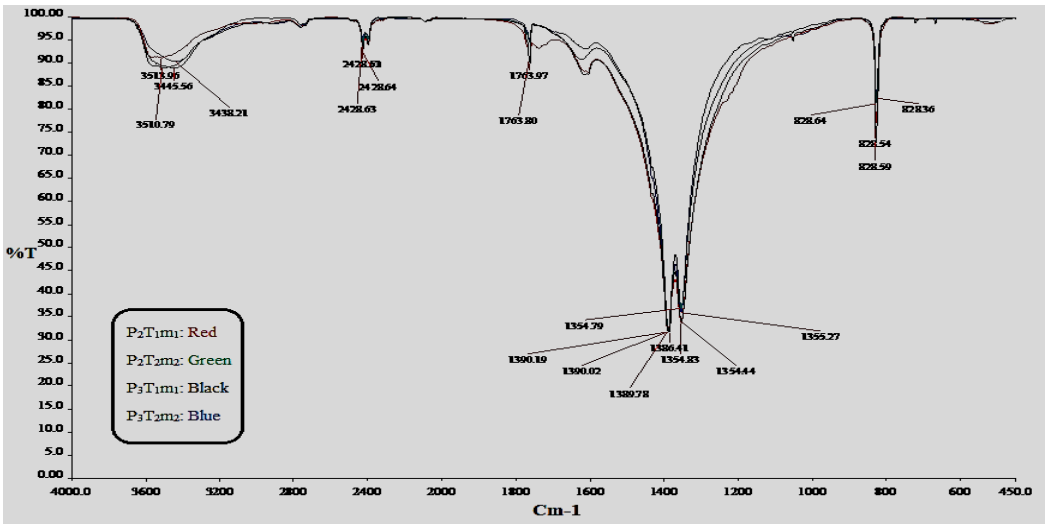


Figure 3. FTIR spectra of cotton cellulose and synthesized cellulose/Zn nanocomposite aerogel samples ($P_2T_1M_1$, $P_2T_2M_2$, $P_3T_1M_1$, and $P_3T_2M_2$).

Overall, the FTIR results indicate that the cellulose matrix retained its fundamental chemical structure after composite formation, while interacting with the Zn-containing species. However, FTIR alone does not provide direct evidence for nitrate reduction or definitive identification of all Zn-containing phases. Rather, the spectra support the incorporation and confinement of Zn-containing species within the cellulose network.

3.2. Crystalline Structure Analysis (XRD)

The crystalline structure of the prepared porous cellulose/Zn-containing composites was examined by X-ray diffraction (XRD) using Cu Kα radiation (λ = 1.5406 Å) operated at 40 kV and 20 mA. Diffraction patterns were collected over the 2θ range of 0-80°. The XRD patterns of the prepared samples are shown in Figure 4, and the corresponding diffraction parameters are summarized in Table 2. All samples exhibited a broad diffraction feature centered at around 2θ ≈ 22.5°, which is characteristic of the cellulose-based matrix, together with sharper reflections associated with Zn-containing crystalline phases. The presence and position of these reflections indicate that the crystalline phase composition was affected by the synthesis conditions. In particular, peaks observed at 2θ values of 15.47°, 18.35°, 33.88°, 36.93°, 39.48°, and 52.95° suggest the formation of different Zn-containing crystalline species within the porous cellulose framework. In general, sharper and more intense reflections indicate the formation of larger crystallite domains, whereas broader peaks are associated with smaller crystallites and/or lower structural order. The crystallite size of the Zn-containing phase was estimated using the Debye-Scherrer equation:

$$D = \frac{K\lambda}{\beta\cos\theta}$$

where D is the crystallite size, K is the shape factor, λ is the X-ray wavelength, β is the full width at half maximum (FWHM) of the selected diffraction peak, and θ is the Bragg angle. As summarized in Table 2, the crystalline characteristics of the prepared composites were strongly dependent on the synthesis conditions. The reflections observed for the P1 series can be tentatively assigned to $Zn(OH)_2$, whereas those in the P_2 and P_3 series may be indexed to ZnO and ZnO_2 related phases, suggesting a change in the Zn-containing crystalline species with processing conditions. In the $P_2T_2M_2$ sample, the diffraction pattern indicates the coexistence of more than

one crystalline phase. A clear inverse relationship between FWHM and calculated crystallite size was observed. The P_1 samples showed relatively low FWHM values (0.19-0.20°) and the largest crystallite sizes, reaching 40.1 nm for $P_1T_1M_1$ and 42.5 nm for $P_1T_2M_2$. In contrast, the P_2 and P_3 samples exhibited broader peaks, with FWHM values ranging from 0.46 to 0.59°, corresponding to smaller crystallite sizes in the range of approximately 14.9-19.1 nm. The smallest crystallite size was obtained for $P_3T_2M_2$ (14.9 nm), which also showed the highest FWHM value (0.59°).

Table 2. XRD parameters and estimated crystallite sizes of the composite samples.

Sample	Tentative Phase	Position (2θ, °)	FWHM (°2θ)	Intensity (cts)	D (nm)
$P_1T_1M_1$	Zn (OH)2	15.47	0.20	128	40.1
$P_1T_2M_2$	Zn (OH)2	18.35	0.19	319	42.5
$P_2T_1M_1$	ZnO	33.88	0.52	33	16.1
$P_2T_2M_2$	Zn / ZnO2*	39.48 / 36.93	0.25 / 0.46	72 / 57	34.8 / 19.1
$P_3T_1M_1$	ZnO2	52.95	0.55	57	16.4
$P_3T_2M_2$	ZnO2	36.91	0.59	48	14.9

*Multiphase coexistence observed.

Note: Crystallite size (D) was estimated using the Debye–Scherrer equation.

These findings are consistent with the SEM and TGA results and further support the presence of Zn-containing crystalline phases within the porous cellulose-based matrix. The smaller crystallite sizes observed in the P_2 and P_3 series may be associated with restricted crystal growth within the cellulose-derived porous network. Overall, the XRD results indicate that the crystalline features of the composites can be tuned by changing the preparation conditions, which may subsequently influence their structural and thermal behavior.

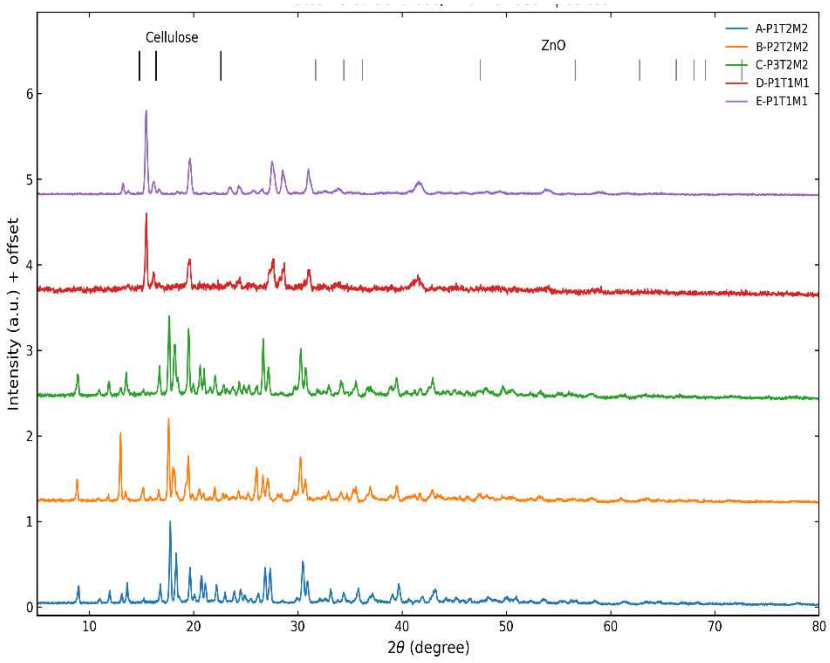


Figure 4: X-ray diffraction (XRD) patterns of the prepared cellulose/Zn-containing composite aerogels. All patterns show the characteristic broad cellulose diffraction band around 2θ ≈ 22.5°, together with sharper reflections associated with Zn-containing crystalline phases. The stacked presentation facilitates comparison of phase evolution among samples prepared under different synthesis conditions

Figure 4 displays the stacked X-ray diffraction (XRD) patterns of the synthesized cellulose/Zn-containing composite aerogels. All patterns exhibit a characteristic broad diffraction feature centered at around $2\theta \approx 22.5°$, which is typically attributed to the amorphous-to-semi-crystalline framework of the cellulose matrix. Superimposed on this broad baseline, several distinct reflection peaks are observed within the 2θ ranges of approximately 15°–20°, 30°–40°, and 50°–60°, suggesting the presence of crystalline Zn-containing species within the porous network. The stacked visual presentation highlights notable variations in peak intensity and line broadening as a function of processing conditions. Based on peak positions and literature comparison, the observed reflections can be tentatively indexed to $Zn(OH)_2$, ZnO, and related Zn-containing phases, as listed in Table 2. Samples prepared under milder synthetic conditions (such as the P_1 series) exhibit relatively sharp and intense reflections, corresponding to larger apparent crystallite sizes (up to ~42.5 nm). In contrast, the P_2 and P_3 series display broader diffraction peaks with higher FWHM values (reaching 0.59°), pointing toward smaller crystallite domains (down to ~14.9 nm for $P_3T_2M_2$) or reduced short-range structural ordering, likely caused by spatial confinement during crystal growth inside the cellulose channels. Overall, these XRD findings are in general agreement with the morphological (SEM) and thermal (TGA) observations, supporting the influence of synthesis parameters on the inorganic phase assembly within the composite network.

.3.3. Morphological and Elemental Characterization

SEM analysis was performed to evaluate the surface morphology of the prepared porous cellulose/Zn-containing composite. As illustrated in Figure 5, the sample showed a porous and heterogeneous microstructure with Zn-containing particulate features distributed throughout the cellulose-based matrix. These features were observed with sizes ranging from approximately 15 to 130 nm. EDS analysis (Figure 6) revealed O, Zn, and N as the principal detected elements in the analyzed region. The presence of Zn supports the incorporation of Zn-containing species into the composite, whereas the N signal provides supporting evidence for the nitrate-containing PCM. The Au peaks are attributed to the gold coating applied prior to SEM analysis. Taken together, the SEM and EDS results confirm the successful formation of a Zn-containing porous cellulose-based composite and are consistent with the structural characteristics observed in the other analytical results.

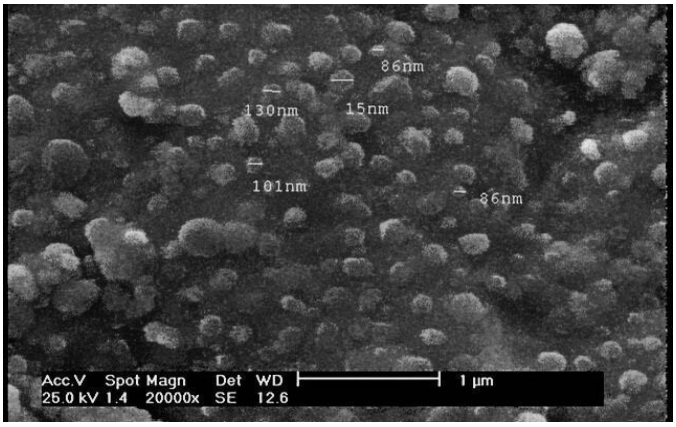


Figure 5. SEM micrograph of the porous cellulose/Zn-containing composite (sample $P_2T_2M_2$), illustrating the surface morphology and dispersed Zn-containing particulate features within the cellulose-based matrix.

The SEM micrograph of sample $P_2T_2M_2$ reveals a porous and heterogeneous surface morphology, indicative of a cellulose-based composite framework with developed void structure. Zn-containing

particulate features are observed throughout the matrix, with approximate sizes in the range of 15–130 nm. These observations suggest the incorporation of Zn-containing domains within the porous cellulose network.

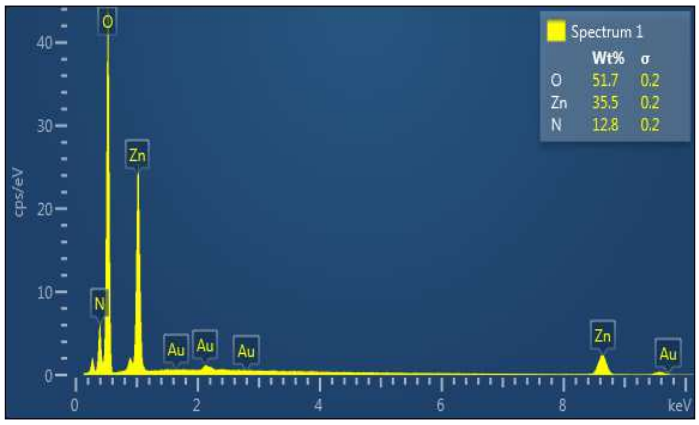


Figure 6. Elemental composition and EDS spectrum of the porous cellulose/Zn-containing composite (sample $P_2T_2M_2$).

The EDS spectrum provides qualitative elemental support for this interpretation by confirming the presence of Zn in the analyzed region, together with O as a major constituent of the cellulose-based structure. The detected N signal may be associated with the nitrate-containing PCM embedded within the composite matrix, while the Au peaks arise from the gold coating applied prior to SEM examination. Overall, the SEM and EDS results are consistent with the formation of a porous cellulose/Zn-containing composite and support the structural features inferred from the complementary characterization analyses.

3.4. Thermal Stability Analysis (TGA)

The thermal stability of neat cotton cellulose and the $P_2T_2M_2$ composite was evaluated by thermogravimetric analysis under a nitrogen atmosphere, and the corresponding curves are presented in Figure7. As observed, neat cotton cellulose shows the characteristic thermal degradation behavior of cellulosic materials, with the major weight-loss step occurring within the intermediate temperature region as a result of depolymerization and decomposition of the polysaccharide backbone. By contrast, the $P_2T_2M_2$ composite displays a clear improvement in thermal resistance, as evidenced by the displacement of the main degradation region toward higher temperatures and the higher residual mass retained at 600 °C.

This enhanced thermal behavior can be attributed to the incorporation of the Zn-containing phase within the cellulose-based porous structure. The inorganic component likely acts as a thermally stabilizing domain that restricts chain mobility, suppresses the release of volatile degradation products, and promotes the formation of a more stable carbonaceous char during heating. The higher char yield of the composite further supports the assumption that the Zn-containing phase contributes to the development of a protective residue, which retards the progress of thermal decomposition.

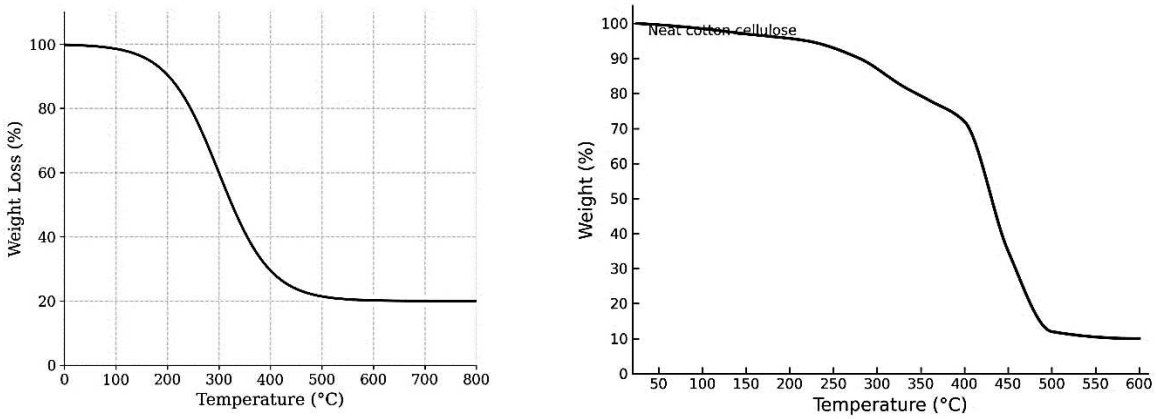


Figure 7. TGA curves of neat cotton cellulose and $P_2T_2M_2$ under nitrogen, showing enhanced thermal stability and char yield of the composite.

Compared with neat cotton cellulose, the $P_2T_2M_2$ composite exhibited a shift in the main degradation region toward higher temperatures, together with a higher residual mass at 600 °C. These findings indicate that the Zn-containing phase modified the thermal degradation pathway of cellulose, delayed its decomposition, and promoted char formation. The resulting improvement in thermal resistance may be beneficial for porous functional materials operating under elevated-temperature conditions.

3.5. Differential Scanning Calorimetry (DSC) Analysis

The thermal energy storage performance and phase transition characteristics of the optimized porous cellulose/Zn-containing composite (sample $P_2T_2M_2$) were systematically investigated via differential scanning calorimetry (DSC); the results are illustrated in Figure 8. The DSC thermogram reveals multiple endothermic transitions, confirming the effective integration of the phase change material (PCM) within the porous cellulose-based matrix containing Zn-derived species. The primary endothermic peak commences at 28.8 °C and reaches its maximum at 39.05 °C, which is ascribed to the melting of the incorporated PCM. The enthalpy of fusion ΔH) was determined to be 157.1 J/g, signifying a substantial latent heat storage capacity and indicating that the PCM preserves its phase-change functionality within the composite architecture. A secondary broad endothermic transition was observed in the 63.2–152 °C range ΔH = 421 J/g. This thermal event is likely associated with structural relaxation, the desorption of physically bound species, and/or thermally induced conformational changes within the composite matrix. Furthermore, a high-temperature endothermic event was detected within the 280.9–345.2 °C range ΔH = 243.7 J/g, corresponding to the thermal decomposition of the cellulose framework and the breakdown of structurally ordered domains. This finding corroborates the TGA results, which likewise indicate the onset of significant structural degradation within this temperature regime. Notably, the incorporation of the Zn-containing nanophase shifts the onset of thermal degradation to approximately 345 °Ca substantial improvement compared to neat cotton cellulose (ca. 315 °C). In summary, these results demonstrate that the synthesized porous cellulose/Zn-containing composite effectively combines significant latent heat storage capacity with enhanced thermal stability, validating its potential for advanced energy-management applications.

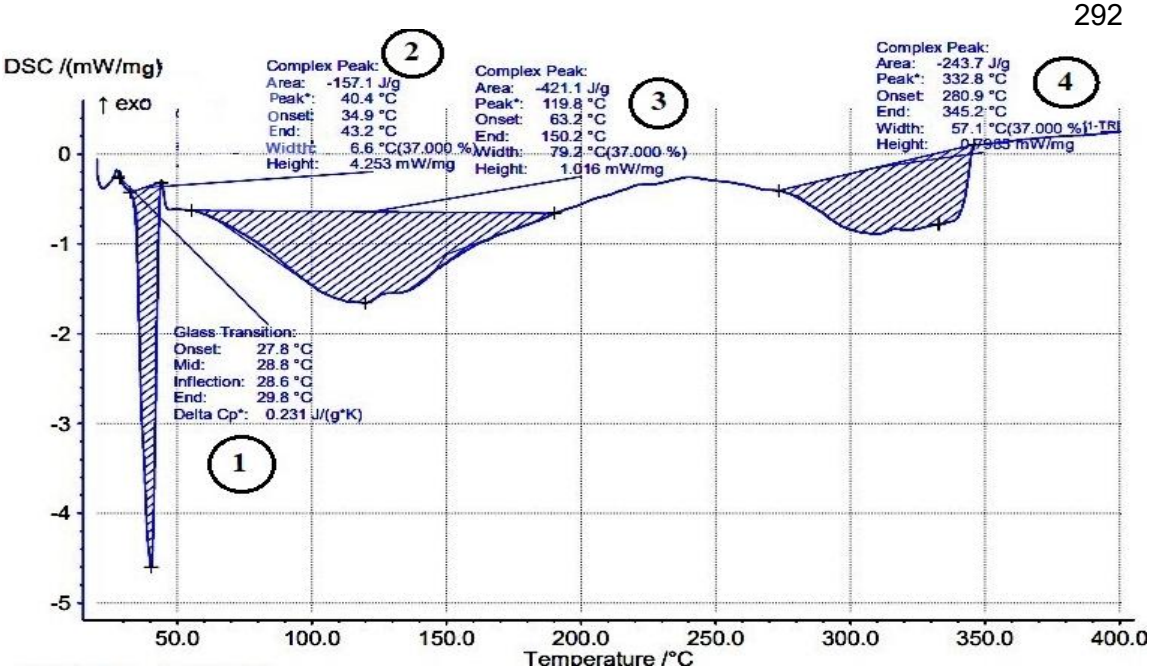


Figure 8. DSC analysis of cellulose/Zn nanocomposite aerogel sample $P_2T_2M_2$

Overall, the obtained results indicate that the developed porous cellulose/Zn-containing composite is a promising candidate for thermal energy storage applications. However, further investigation involving quantitative porosity analysis, leakage assessment, and repeated thermal cycling is required to more comprehensively evaluate its structural integrity, PCM retention capability, and long-term performance under practical operating conditions.

4. Conclusion

In this study, a freeze-dried porous cellulose/Zn-containing composite incorporating zinc nitrate hexahydrate was successfully developed as a bio-based support for low-temperature thermal energy storage applications. Structural and compositional analyses indicated that the cellulose-derived porous framework effectively accommodated Zn-containing crystalline species and promoted their distribution within the composite matrix. FTIR results suggested interactions among cellulose functional groups, nitrate ions, and Zn-containing species, while XRD confirmed the presence of Zn-containing crystalline phases formed under the applied processing conditions. SEM/EDS observations further supported the porous morphology of the scaffold and the presence of Zn-containing particulate domains distributed throughout the cellulose matrix. Thermal analyses demonstrated that the composite exhibited improved thermal stability compared with neat cellulose, as reflected by the shift of the main degradation region toward higher temperatures and the formation of a higher residual mass after thermal treatment. Differential scanning calorimetry showed that the optimized sample ($P_2T_2M_2$) possessed a latent heat storage capacity of 157.1 J/g and a peak melting temperature of 39.05 °C, indicating its potential suitability for low-temperature thermal energy storage systems. Overall, the findings suggest that freeze-dried porous cellulose/Zn-containing composites are promising sustainable support materials for hydrated-salt phase change systems. Nevertheless, further investigations including quantitative porosity analysis, leakage resistance evaluation, and long-term thermal cycling tests are necessary to fully assess their practical applicability and long-term performance.

Declaration of Interest

The authors declare that they have no known competing financial interests or personal relationships that could have appeared to influence the work reported in this paper.

Data Availability Statement

The data that support the findings of this study are available from the corresponding author upon reasonable request.

References

[1] Kistler, S. (1931). Coherent expanded aerogels and jellies. Nature, 127(3214), 741.

[2] Kistler, S. (1932). Coherent Expanded Aerogels. Rubber Chemistry and Technology, 5(4), 600–603.

[3] Zhang, S., Huang, X., Feng, J., Qi, F., Dianyu, E., Jiang, Y., Li, L., & Xiong, S. (2020). Structure, compression and thermally insulating properties of cellulose diacetate-based aerogels. Materials & Design, 189, 108502.

[4] Sun, X., Ji, S., Wang, M., Dou, J., Yang, Z., Qiu, H., Kou, S., Ji, Y., & Wang, H. (2020). Fabrication of porous TiO2TiO_2TiO2-RGO hybrid aerogel for high-efficiency, visible-light photo degradation of dyes. Journal of Alloys and Compounds, 819, 153033.

[5] Kaya, G., & Deveci, H. (2020). Synergistic effects of silica aerogels/xerogels on properties of polymer composites: A review. Journal of Industrial and Engineering Chemistry, 89, 13–27.

[6] Zhang, Z., Tan, J., Gu, W., Zhao, H., Zheng, J., & Zhang, B. (2020). Cellulose-chitosan framework/polyailine hybrid aerogel toward thermal insulation and microwave absorbing application. Chemical Engineering Journal, 395, 125190.

[7] Ge, N., Hu, X., Pan, Z., Cai, S., Fu, F., Wang, Z., Yao, J., & Liu, X. (2023). Sustainable fabrication of cellulose aerogel embedded with ZnO@noble metal (Ag, Au, Ag-Au) NPs for sensitive and reusable SERS application. Colloids and Surfaces A: Physicochemical and Engineering Aspects, 671, 131650.

[8] Pang, C., You, H., Liang, L., Li, Z., Lin, X., Zhang, Y., Zhang, H., Pan, X., Hu, Y., Chen, Y., Luo, X., & Wang, H. (2023). Bamboo pulp-based electret fiber aerogel for simulated radioactive aerosol purification. Colloids and Surfaces A: Physicochemical and Engineering Aspects, 658, 130502.

[9] Wang, J., Yi, D., Peng, X., Yang, H., Wang, T., Gao, J., Xie, B., & Su, G. (2022). The hydrophobically modified cellulose-based aerogel loaded with BTA enhances the anticorrosion properties of epoxy coating. Colloids and Surfaces A: Physicochemical and Engineering Aspects, 653, 129835.

[10] He, S., Liu, A., Zhang, J., Liu, J., & Shao, W. (2022). Preparation of ε\varepsilonε-polylysine and hyaluronic acid self-assembled microspheres loaded bacterial cellulose aerogels. Colloids and Surfaces A: Physicochemical and Engineering Aspects, 654, 130114.

[11] Shi, W., Ching, Y., & Chuah, C. (2021). Preparation of aerogel beads and microspheres based on chitosan and cellulose for drug delivery: A review. International Journal of Biological Macromolecules, 170, 751–767.

[12] Dai, Y., Jing, Z., Li, Z., Zhu, Y., Qiu, F., Pan, J., Zhang, T., & Li, C. (2022). Efficient cellulose aerogel biosorbents functionalized by nanosized zero-valent iron. Colloids and Surfaces A: Physicochemical and Engineering Aspects, 651, 129765.

[13] Shang, Q., Cheng, J., Hu, L., Bo, L. Y., Yang, X., Hu, Y., Liu, C., & Zhou, Y. (2022). Bio-inspired castor oil modified cellulose aerogels for oil recovery and emulsion separation. Colloids and Surfaces A: Physicochemical and Engineering Aspects, 636, 128043.
[14] Ma, Z., Han, Y., Xing, X., Zhu, H., Wang, Q., & Wang, X. (2022). Preparation of micro-convex rough interface carbon aerogels with cellulose-lithium bromide (LiBr) molten salt hydrate gelled system. Colloids and Surfaces A: Physicochemical and Engineering Aspects, 650, 129624.
[15] Lin, J., Du, Y., Ma, X., Li, Y., Xie, H., Qi, Y., & Zhang, S. (2023). Choline chloride/urea etched carbon fiber to improve the elasticity of biomass-based carbon aerogel. Colloids and Surfaces A: Physicochemical and Engineering Aspects, 669, 131506.
[16] Aegerter, M. A., Leventis, N., & Koebel, M. A. (2011). Aerogels Handbook. Springer.
[17] Wei, D. W., Wei, H., Gauthier, A. C., Song, J., Jin, Y., & Xiao, H. (2020). Superhydrophobic modification of cellulose and cotton textiles: Methodologies and applications. Journal of Bioresources and Bioproducts, 5(1), 1–15.
[18] Thomas, B., Raj, M. C., Athira, K. B., Rubiyah, M. H., Joy, J., Moores, A., Drisko, G. L., & Sanchez, C. (2018). Nanocellulose, a versatile green platform: from biosources to materials and their applications. Chemical Reviews, 118(23), 11575–11625.
[19] Budtova, T. (2019). Cellulose II aerogels: A review. Cellulose, 26(1), 81–121.
[20] Zaman, A., Huang, F., Jiang, M., Wei, W., & Zhou, Z. (2020). Preparation, Properties, and Applications of Natural Cellulosic Aerogels: A Review. Energy and Built Environment, 1(2), 60–76.
[21] Korhonen, O., & Budtova, T. (2020). All-cellulose composite aerogels and cryogels. Composites Part A: Applied Science and Manufacturing, 137, 106027.
[22] Wang, Z., Zhu, W., Huang, R., Zhang, Y., Jia, C., Zhao, H., Chen, W., & Xue, Y. (2020). Fabrication and Characterization of Cellulose Nanofiber Aerogels Prepared via Two Different Drying Techniques. Applied Sciences, 10(12), 4271.
[23] Li, M., Jiang, H., & Xu, D. (2018). Synthesis and characterization of a xonotlite fibers–silica aerogel composite by ambient pressure drying. Journal of Porous Materials, 25(5), 1417–1425.
[24] Missfeldt, F., Gurikov, P., Loelsberg, W., Weinrich, D., Lied, F., Fricke, M., & Smirnova, I. (2020). Continuous supercritical drying of aerogel particles: Proof of concept. Industrial & Engineering Chemistry Research, 59(26), 11284–11295.
[25] El-Naggar, M. E., Othman, S. I., Allam, A. A., & Morsy, O. M. (2020). Synthesis, drying process and medical application of polysaccharide-based aerogels. International Journal of Biological Macromolecules, 145, 1115–1128.